ELSEVIER

Journal of Crystal Growth 237–239 (2002) 154–158

JOURNAL OF CRYSTAL GROWTH

www.elsevier.com/locate/jcrysgro

2D and 3D phase-field simulations of lamella and fibrous eutectic growth

M. Apel*, B. Boettger, H.-J. Diepers, I. Steinbach

ACCESS eV, Intzestrasse 5, D-52072 Aachen, Germany

Abstract

The coupled eutectic growth of binary alloys was studied by means of phase-field models or boundary integral methods for many years. The use of numerical methods discovered the remarkable variety of growth structures like lamellae or different kinds of oscillating modes. In this work, the multi-phase-field method which is generally valid for most kinds of transitions between multiple phases is applied to the eutectic growth problem. We simulated the directional solidification of a binary eutectic during the initial transient state in 2 and 3 dimensions. The chosen phase diagram of the eutectic alloy is asymmetric with a composition ratio between the two solid phases α and β of 0.82. The 2D simulations show stable lamella growth or unstable oscillating modes dependent on the number of β lamella specified by explicit seeding at the bottom of the calculation domain. The undercooling at the growth front is evaluated for different spacing and compared with the values obtained by the fundamental analysis for the steady-state growth via the Jackson and Hunt model. For the regular lamella growth, the undercooling evaluated from the phase-field simulations fits within 20% of the analytical values. 3D calculations show the fibrous growth structure. This is in agreement with the expectation because for small phase fractions of β the fibrous structure possesses a smaller total amount of surface energy compared with lamellas and therefore should be preferred. For a larger number of fibres, they tend to form a hexagonal arrangement which is usually observed by experiments.

PACS: 81.10.Aj; 1.10.Fg; 64.70.Dv

Keywords: A1. Crystal morphology; A1. Directional solidification; A1. Eutectics; A1. Growth models

1. Introduction

Reduction of total free energy is the basic driving force of any phase transformation process. Based on this principle, the phase-field method has been applied to simulate microstructure evolution during materials processing [1–5]. The applications reach from the investigation of morphological instabilities, e.g. dendritic growth to structural phase transitions in solid–solid systems. Several phase-field or boundary integral methods already exist for the simulation of eutectic solidification [6–9,13]. The multi-phase-field method [10,11] is a natural extension of the basic phase-field concept to the interaction of more than two individual phases. It offers the perspective for the simulation of ternary and higher order eutectics as well.

*Corresponding author. Tel.: +49-241-80-6721; fax: +49-241-38578.

E-mail address: m.apel@access.rwth-aachen.de (M. Apel).

0022-0248/02/$ - see front matter
PII: S0022-0248(01)01895-4

In this paper, we will apply the multi-phase-field method to eutectic solidification of a binary alloy but further development will be directed towards multi-component and multi-phase systems.

2. The multi-phase-field model

We consider a system of N field variables $\phi_{\alpha(\vec{x},t)}$, $\alpha = 1, \ldots, N$, $0 \leqslant \phi_\alpha \leqslant 1$. In our context, these variables may be identified with the local phase state (liquid or solid matrix) but several individual grains of a one solid phase identified by their orientation can exist. In the bulk of one grain α $\phi_\alpha = 1$ holds, on grain boundaries between grain α and grain β $\phi_\alpha + \phi_\beta = 1$ and $\phi_\alpha < 1$, $\phi_\beta < 1$. In general, the sum over all phases equals 1.

We use the approach described in Ref. [11] which leads to a set of phase-field equations for each field variable ϕ_α

$$\dot{\phi}_\alpha = \sum_{\beta \neq \alpha} \mu_{\alpha\beta} \left\{ \sigma_{\alpha\beta} \left[(\phi_\beta \nabla^2 \phi_\alpha - \phi_\alpha \nabla^2 \phi_\beta) + \frac{\pi^2}{2\eta^2}(\phi_\alpha - \phi_\beta) \right] + \frac{\pi}{\eta} \sqrt{\phi_\alpha \phi_\beta} \Delta G_{\alpha\beta} \right\}. \quad (1)$$

The constants are: $\sigma_{\alpha\beta}$ is the boundary energy (J/cm^2), $\eta_{\alpha\beta}$ the boundary thickness (cm), $G_{\alpha\beta}$ the enthalpy difference between the bulk phases (J/cm^3) and $\mu_{\alpha\beta}$ the mobility of boundary (cm^4/Js). In Eq. (1), we have set all boundaries to the same thickness $\eta_{\alpha\beta} = \eta$ and neglected higher order triple point contributions [10,11].

Coupling with concentration c (for details see Ref. [3]) occurs only via the difference in the Gibbs free energy $\Delta G(c)$ which is expressed by a linear relationship $\Delta G = \Delta S_f \ (T^{eq}(c) - T)$. T^{eq} denotes the equilibrium temperature for a given composition and can be derived from the phase diagram. T is the actual temperature. We describe solute diffusion by a mixture composition description

$$\dot{c} = \sum_{i=1}^{N} \nabla \Phi_i D_i \nabla c_i, \quad (2)$$

where c_i denotes the concentration in phase i with its diffusion coefficient D_i. Within the interfaces, local equilibrium according to

$$c_i = k_{ij} c_j, \quad \forall i,j \quad (3)$$

is set. k_{ij} denotes the partition coefficient between the two phases i and j. Within the bulk of each phase Eq. (2) simplifies to Fix's second law.

3. Simulation results

Based on the multi-phase-field model described above we have simulated the solidification of a binary eutectic model alloy with the two solid phases α and β. We choose an asymmetric phase diagram with an α/β ratio of 0.82. Solidus and liquidus lines are defined by their slopes at the eutectic point: $m_{\alpha sol} = -100\,\mathrm{K/at\%}$, $m_{\alpha liq} = -10\,\mathrm{K/at\%}$ and $m_{\beta sol} = 100\,\mathrm{K/at\%}$, $m_{\beta liq} = 5\,\mathrm{K/at\%}$. Temperature is normalized to the eutectic temperature. Eutectic composition is set to $c_{Eut}/c_\beta = 0.2$, $c_\beta = 5\,\mathrm{at\%}$. Diffusion coefficient in the melt is set to $10^{-5}\mathrm{cm}^2/\mathrm{s}$ and we neglect diffusion in the solid. The surface energy is $10^{-5}\mathrm{J/cm}^2$ for all interfaces. All simulations were performed for directional solidification conditions, e.g. constant temperature gradient (50 K/cm) and cooling rate (0.005 K/s). To save computer time, we implemented a moving grid algorithm which adapts the calculation domain to the moving solid–liquid interface.

As initial conditions for the simulation we have set a fixed number of β-nuclei embedded in the α-matrix at arbitrary positions at the bottom of the calculation domain. The number of nuclei defines the minimal spacing λ within one simulation run because the nucleation of new grains is not taken into account. Adjustment to larger λ values is possible since individual lamella can disappear.

Fig. 1a shows a result for a 2D simulation run with 14 initial β nuclei. A stable lamella growth structure with $\lambda = 25\,\mu\mathrm{m}$ has been established after 400 μm of solidification. We measured the spacing by evaluating the distances between isolines in the concentration field for every cutting plane normal to the growth direction. From the plot of the variance $\sigma_{\langle\lambda\rangle}$ in the distribution of the lamella distances against the height of the cutting plane, the oscillation frequency and the stability of the

growth mode can be derived (see Fig. 2b). Since we start with an arbitrary lamella configuration even the stable spacing shows oscillations in the transient stage but the amplitude decreases steadily. The decrease in amplitude clearly indicate stable growth for the spacing of $\lambda = 25\,\mu m$.

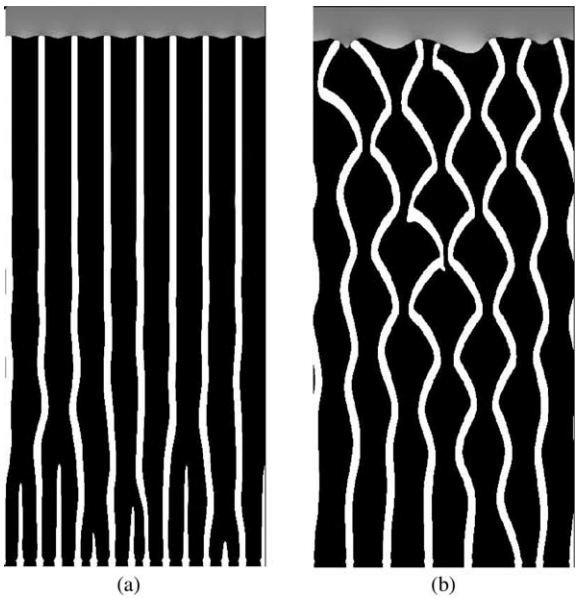

Fig. 1. (a) Stable lamella growth and (b) oscillating growth mode. The concentration is colour coded. White represents β phase, black the α phase. Size of the whole calculation domain is $200\,\mu m \times 426\,\mu m$. Growth velocity is $1\,\mu m/s$.

Fig. 1b shows the result for 7 initial β nuclei. Now the oscillation amplitude increases during the first stages of the solidification. At the end of the simulation run it turned out to be saturated but a longer simulation time would be necessary to prove this. The oscillation period of $12.5\,\mu m$ for the unstable case, derived by fitting the curves in Fig. 2b, is larger than that for the stable growth which is $10.7\,\mu m$. Their ratio of 1.17 is nearly the ratio of the mean spacing which is 1.14. Since lateral diffusion accounts for the oscillation an increasing period can be expected for larger mean spacing.

For the solid–liquid interface, we derived in the case of Fig. 1(a) an average undercooling of $\Delta T = 0.11\,K$ at the end. Compared to this value the calculation after Jackson and Hunt [12] gives for the interface undercooling a value of $\Delta T = 0.13\,K$ which is an agreement within 20%.

According to the JH-analysis a fixed value of λ is correlated with a fixed interfacial undercooling. Slight variations of λ can be obtained in the simulation by varying the domain width for a constant number of initial seeds. Stable lamella growth was observed for λ between 19 and $25\,\mu m$ (Fig. 2a). The transition between stable and oscillating growth takes place for $\lambda > 26\,\mu m$. Simultaneously, the interface undercooling varies with $\lambda\cdot$ For the undulated interface in the case of the oscillating mode the undercooling is between 0.1 and 0.18 K along the interface. It exceeds the

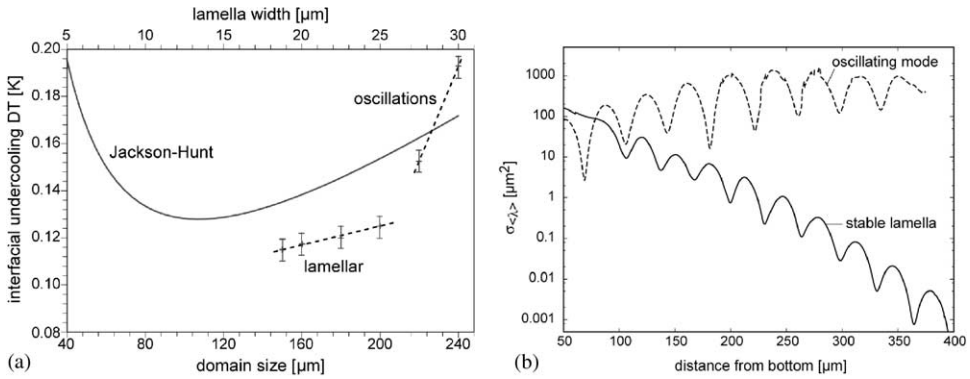

Fig. 2. (a) Interface undercooling as a function of lamella width, respectively, domain size. Line: Jackson–Hunt model. Symbols: Phase-field simulations. For lamella width $> 25\,\mu m$ a transition of stable lamella growth to oscillating growth occurs. (b) Standard deviation σ of the mean lamella spacing as a function of growth height for the structures shown in Fig. 1. For stable growth initial oscillations decrease.

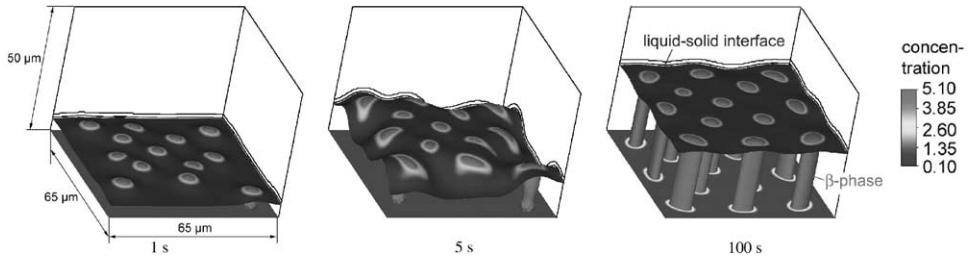

Fig. 3. Fibrous structure obtained in 3D after 1, 5, 100 s of growth. The initial stage has an undulated solid–liquid interface because the spacing is far from the stable distance. The surface becomes smoother when it tends towards the steady state.

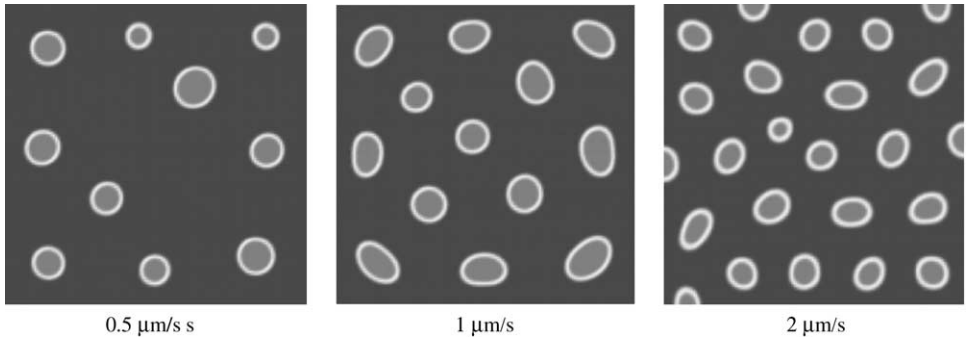

Fig. 4. Top view on the 3D growth structures for three different growth velocities 0.5, 1, 2 µm/s. With increasing velocity the structure becomes finer and the array tends towards a hexagonal arrangement.

maximum value of ~ 0.12 K for stable growth (see Fig. 2a).

For the chosen type of asymmetric phase diagram with a α/β phase fraction ratio of 0.82 fibrous growth will be expected instead of lamella structures. Fig. 3 shows the simulated structure for 1, 5 and 100 s of growth. All simulation parameters are the same as for the simulation run shown in Fig. 1(a) except for the dimensions of the calculation domain and the arrangement of the β seeds. As expected a fibre structure occurs. The large undulated solid–liquid interface can be clearly seen in the initial stages. After 100 s a FCC array with 13 β fibres has been formed. The mean distance between the fibres is in this case $\lambda = 18\,\mu$m. This is smaller than $\lambda = 25\,\mu$m for the 2D case. It must be noted that in the 3D case the constrains due to the boundary conditions are larger which certainly effects the selection of the spacing. This can be seen in Fig. 4, where the arrangement for three different growth velocities is shown. For the largest velocity of 2 µm/s a finer structure with 21.5 fibres has been formed after 100 s. For this larger number of fibres the array tends more towards a hexagonal arrangement which is usually observed by experiments.

Acknowledgements

This work was supported by Deutsches Zentrum für Luft—und Raumfahrt (DLR) under grant No. 50WM0043.

References

[1] G.J. Fix, in: A. Fasano, M. Primicerio (Eds.), Free Boundary Problems: Theory and Applications, Vol. II, Piman, Boston, 1983, p. 580.

[2] A.A. Wheeler, W.J. Boettinger, G.B. Mc Fadden, Phys. Rev. E 47 (1993) 1893.
[3] J. Tiaden, B. Nestler, H.J. Diepers, I. Steinbach, Physica D 115 (1998) 73.
[4] H.J. Diepers, C. Beckermann, I. Steinbach, Acta Mater. 47 (1999) 3663.
[5] C. Beckermann, H.J. Diepers, I. Steinbach, A. Karma, X. Tong, J. Comp. Phys. 154 (1999) 468.
[6] B. Nestler, A.A. Wheeler, Physica D 138 (2000) 114.
[7] M. Plapp, W.J. Boettinger, S.R. Coriell, A.L. Greer, A. Karma, W. Kurz, M. Rappaz, R. Trivedi, Acta Mater. 48 (2000) 43.
[8] M. Apel, M. Seeßelberg, J. Tiaden, in: R. Stauber, et al. (Eds.), Werkstoffwoche/Materialica, 1998, Vol. 6, Wiley-VCH, Weinheim, 1999, pp. 755–760.
[9] I. Steinbach, F. Pezzolla, B. Nestler, M. Seeßelberg, R. Prieler, G.J. Schmitz, J.L.L. Rezende, Physica D 94 (1996) 135–147.
[10] K. Kassner, A. Valance, C. Misbah, D. Temkin, Phys. Rev. E 48 (2) (1993) 1091.
[11] I. Steinbach, F. Pezzolla; Physica D 134 (1999) 385.
[12] A. Jackson, D.J. Hunt, TMS AIME 236 (1966) 1129.
[13] A. Karma, A. Sarkissian, Met. Mater. Trans. A 27A (1996) 635.